Journal of Sol-Gel Science and Technology (2019) 90:281–295
https://doi.org/10.1007/s10971-019-04960-1

ORIGINAL PAPER: FUNCTIONAL COATINGS, THIN FILMS AND MEMBRANES (INCLUDING DEPOSITION TECHNIQUES)

Modification in the microstructural and electrochromic properties of spray-pyrolysed WO_3 thin films upon Mo doping

Anil Kumar[1] · Chandra Shekhar Prajapati[2] · P. P. Sahay[1]

Received: 4 January 2019 / Accepted: 5 March 2019 / Published online: 14 March 2019

Abstract

WO_3 thin films were grown onto the glass and fluorine-doped tin oxide-coated glass substrates using chemical spray pyrolysis technique. X-ray diffraction analyses reveal that all the films possess orthorhombic phase of WO_3. Morphologies of the films have been found to vary with Mo-doping concentrations. Three-dimensional atomic force micrographs reveal that the 5 at% Mo-doped film has the maximum image surface area and is optimal for improved electrochromic performance. Cyclic voltammetry studies show that the cathodic and anodic peak current densities have the highest values for the 5 at% Mo-doped WO_3 film. Relative to the undoped film, the change from coloured to bleached state is faster for the 5 at% Mo-doped WO_3 film. Considering the reversibility and the switching response from chronoamperometry and the coloration efficiency from cyclic voltammetry, it has been concluded that the 5 at% Mo-doped WO_3 film has an optimal electrochromic response.

Graphical Abstract

By analysing the results of cyclic voltammetry and chronoamperometry measurements, it has been found that the 5 at% Mo-doped WO_3 film has optimal electrochromic performance.

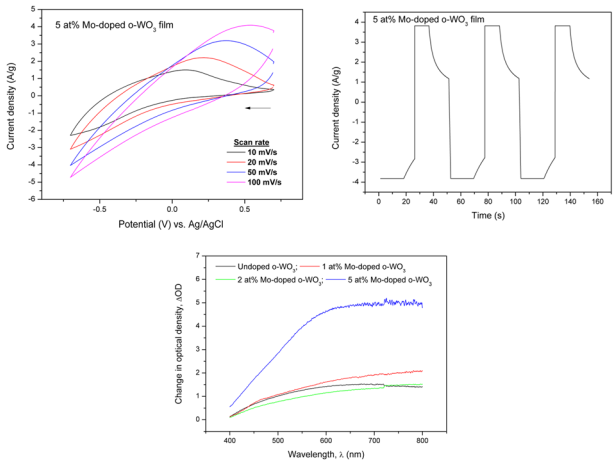

✉ P. P. Sahay
dr_ppsahay@rediffmail.com

[1] Department of Physics, Motilal Nehru National Institute of Technology Allahabad, Allahabad 211004, India

[2] Centre for Nano Science and Engineering, Indian Institute of Science Bangalore, Bengaluru 560012, India

Highlights

- As-deposited films possess orthorhombic phase of WO_3.
- 5 at% Mo-doped WO_3 films have the maximum image surface area.
- WO_3 film doped with 5 at% Mo exhibits fastest switching response.
- 5 at% Mo-doped film exhibits optimal electrochromic performance.

Keywords Mo-doped WO_3 thin films · Cyclic voltammetry · Coloration efficiency · Chronoamperometry · Electrochromism

1 Introduction

Electrochromism is the phenomenon exhibited by certain materials, where the materials reversibly change their colours when they are subjected to an electric field. Reversible change in colour arises when the material undergoes different electronic states during electrochemical redox reactions. The most important feature of electrochromism is that an electric field is required only during the change (colour or bleach process), which can be controlled at any intermediate stage. Owing to persistence and reversible nature of colour change, such materials, called electrochromic materials, are used in smart windows, which control the amount of light and heat passing through them. In addition, electrochromic materials are used to automatically dimming rear-view mirrors in various ambient light conditions, and more recently, in electrochromic displays.

Electrochromic materials belong to both inorganic and organic chemical systems. Inorganic systems include transition metal oxides, phthalocyanine compounds, Prussian blue, etc., whereas organic systems are bipyridilium systems, conducting polymers, etc. [1–6]. Among transition metal oxides, tungsten oxide (WO_3) is the most promising one for electrochromic device applications, and therefore has been widely studied. Kostis et al. [7] have reported the improved electrochromic behaviour of highly porous WO_3 films deposited by the hot wire method combined with rapid injection of oxygen pulses. Bhosale et al. [8] have studied the electrochromic properties of hydrothermally synthesised WO_3 nanoflowers on etched ITO substrates. Li et al. [9] have investigated the electrochromic performance of amorphous tungsten oxide films deposited by DC sputtering. Karuppasamy and Subrahmanyam [10] have studied electrochromic behaviour of sputter-deposited vanadium doped WO_3 thin films.

Various techniques such as pulsed laser deposition [11], spin coating [12], sol–gel [13], electrodeposition [14], sputtering [15], etc. have been employed to prepare WO_3 thin films. In the present work, chemical spray pyrolysis technique being simple in operation and involving low-cost equipment, has been used to grow WO_3 thin films. It is a well established fact that electrochromic performance of the films is closely linked to the microstructural features of the films, which are greatly influenced by the deposition technique, the precursor and the solvent used. Another effective way to alter the microstructural features of the film is the inlay of appropriate dopants in the host lattice network. Although addition of dopants such as V, Ti, Zn, Nb, Ni, Ru, etc. in WO_3 lattice network has been studied for improving the electrochromic behaviour of the films [10, 16–19], but exploration of new dopants as well as less-investigated dopants such as Mo, Gd, etc. in WO_3 lattice network to improve electrochromic performance of the films always remains the subject of great interest to the materials scientists, which is behind the motivation and the driving force for this investigation. Yin et al. [15] have studied the influence of Gd doping on electrochromic behaviour of sputter-deposited WO_3 films and found high coloration efficiency and fast switching response for the Gd-doped film. Karuppasamy and Subrahmanyam [10] have reported that the addition of vanadium to WO_3 thin films decreases coloration efficiency of the films. Paipitak et al. [16] have investigated the influence of Ti and Zn doping on the structural and electrochromic performance of sol–gel-derived WO_3 thin films and found that small doping concentration of Ti improves the electrochromic performance of the films. Influence of Nb doping on the electrochromic properties of spray-deposited WO_3 thin films have been studied by Bathe and Patil [17]. They have reported that the coloration efficiency is decreased upon Nb doping, but the charge storage capacity, reversibility and cycle stability improve for the doped films. Green et al. [18] have studied electrochromism in sputter-deposited Ni_xW_{1-x} oxide films and reported that Coloration efficiency improves for films with $0.10 < x < 0.15$. Cazzanelli et al. [19] have examined the influence of Ru doping on the optical and electrochromic properties of sputter-deposited WO_3 thin films, and found that the presence of Ru ions affects these properties of the films. To the best of our knowledge, there are only a very few investigations on the effect of Mo doping on the electrochromic behaviour of tungsten oxide thin films [20, 21].

León et al. [20] have reported the improved electrochromic behaviour of sprayed WO_3 thin films by Mo doping. Madhavi et al. [21] have found that 1.3 at% Mo doping to sputter-deposited WO_3 thin films improves optical modulation and coloration efficiency of the films. In this paper, we have reported the results on the electrochromic performance of spray-pyrolysed WO_3 thin films upon Mo doping. The novelty of this study is that the host and dopant precursors used here are quite different from those used by earlier researchers [20], resulting in modification in the microstructural and electrochromic properties of the films.

2 Experimental details

Undoped and Mo-doped WO_3 thin films were grown onto the glass and fluorine doped tin oxide (FTO)-coated glass substrates, employing the chemical spray pyrolysis technique. Spray pyrolysis involves the pyrolytic decomposition of a precursor solution when sprayed onto the hot substrate, resulting in the formation of thin films. The host precursor solution used here was ammonium tungstate ($(NH_4)_2WO_4$) dissolved in warm water (60–70 °C). Ammonium tungstate as the host precursor was chosen in the present investigation because first, the decomposition reaction was thermodynamically favourable and no residue of the reactant was left behind in the deposited films; second, the precursor salt was completely dissolved in the warm water without any further chemical treatment; and third, the precursor salt was commercially available and cost-effective. The dopant salt used was molybdenum (V) chloride ($MoCl_5$). All the chemicals were of high purity obtained from Alfa Aesar (U.K.). Prior to deposition, the glass and FTO-coated glass substrates were cleaned thoroughly. The schematic representation of home-made spray pyrolysis set-up has been described elsewhere [22]. The deposition parameters were optimised to grow good quality thin films by controlling the process parameters after several depositions. It has been found that substrate temperature is the most crucial parameter in spray pyrolysis, which was kept at ~390 ± 10 °C. The concentration of host precursor solution was 0.1 M. The electrode area of as-deposited film in each case was 2.5 cm^2. The amounts of tungsten oxide deposited on the substrates were determined with the help of an electronic precision balance (Citizen make; Model CX165). The reproducibility of the films was confirmed by analysing the experimental results of several samples under identical conditions. The formation of WO_3 film can be described by the following chemical reaction [23]:

$$(NH_4)_2WO_4 = WO_3 + 2NH_3 \uparrow + H_2O \uparrow \quad (1)$$

The as-deposited films were subjected to further characterisations of different physical properties. The crystallographic phases of the as-deposited films were determined by X-ray diffraction (XRD) analyses using a Rigaku X-ray diffractometer with $CuK\alpha_1$ ($\lambda = 1.5406$ Å) radiation. The surface morphologies of the films were evaluated using a field-emission scanning electron microscope and an atomic force microscope (AFM). Compositional analyses of the films were carried out by the energy-dispersive X-ray (EDX). The optical transmittance spectra of the films were recorded by employing a Shimadzu UV–Vis–NIR spectrometer (Model: UV 3600 Plus) in the wavelength range of 300–800 nm. The electrochromic behaviour of the films deposited on FTO-coated glass substrates were studied using a three-electrode electrochemical cell configuration with the film as a working electrode, platinum wire as a counter electrode, and Ag/AgCl as a reference electrode. All measurements were taken by means of an Electrochemical Analyser (Model: Autolab PGSTAT101) in the electrolyte of 0.01 M H_2SO_4.

3 Results and discussion

3.1 Structural and morphological studies

3.1.1 XRD analyses

The XRD profiles of the as-deposited films onto FTO-coated glass substrates are shown in Fig. 1. All the films are polycrystalline in nature and possess orthorhombic phase of WO_3 (JCPDS Card No. 71-0131). No phase corresponding to molybdenum or other molybdenum compound is observed in the pattern, indicating that molybdenum gets incorporated into the tungsten oxide lattice. Orthorhombic

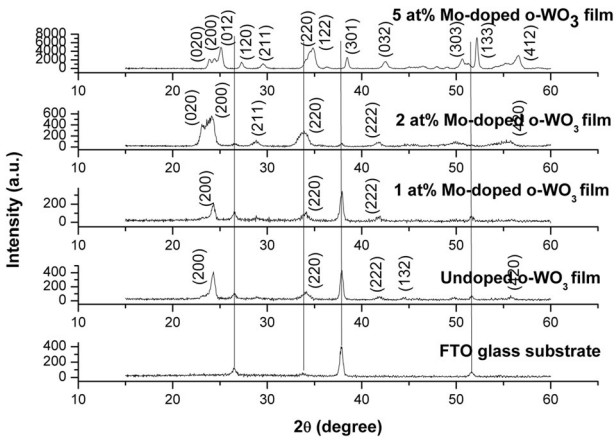

Fig. 1 XRD profiles of WO_3 films

phase of WO_3 has also been reported by Madhavi et al. [20] in the sputtered tungsten oxide films. Rajagopal et al. [24] have observed orthorhombic phase of WO_3 in hydrothermally synthesised WO_3 nanostructures. León et al. [21] have reported the monoclinic phase of WO_3 in spray-pyrolysed tungsten oxide films, where the spray solution used was tungsten chloride (WCl_6) dissolved in dimethylformamide ($HCON(CH_3)_2$). It has been established that WO_3 shows the polymorphism behaviour, i.e., it crystallises in a variety of crystal lattice systems. The basic structure of tungsten oxide consists of WO_6 octahedra shared among several arrangements (edges, corners, and planes) and connected with one another by W–O–W bonds. The structural transformation occurs due to the shifts in the position of W atom in the octahedra, and the changes in the W–O bond lengths [2, 25]. In fact, the polymorphism of WO_3 is influenced considerably by the growth technique as well as process parameters including precursors and solvents used in the technique.

It has been observed that the preferential growth of the film along different lattice planes is closely related to the varying Mo-dopant concentration. The low intensity peaks (132) and (420) observed in the XRD pattern of undoped WO_3 disappear with the addition of 1 at% Mo doping, whereas additional peaks in the XRD pattern are observed upon higher Mo doping. The diffraction peaks corresponding to FTO glass substrate are not seen in the XRD profile of 5 at% Mo-doped WO_3 film. It is inferred that nucleation and growth kinetics of the films are dependent upon Mo doping concentration. The d-spacings corresponding to three most intense peaks observed in the XRD profiles of the films, and the average crystallite size estimated from these peaks using the Scherrer Eq. 2 given below [22] are listed in Table 1. The unit cell parameters (a, b, and c) and the lattice strain (ε) have been determined using the Eq. 3 and the tangent formula (4) given below [22, 26], respectively, and are listed in Table 1.

$$D = \frac{0.9\lambda}{\beta' \cos\theta} \tag{2}$$

$$\frac{1}{d^2} = \frac{h^2}{a^2} + \frac{k^2}{b^2} + \frac{l^2}{c^2} \tag{3}$$

$$\varepsilon = \frac{\beta'}{4\tan\theta} \tag{4}$$

where λ, β' and θ represent the X-ray wavelength, the full width at half maximum (FWHM) of the diffraction peak, and the Bragg's diffraction angle, respectively. Variation observed in the crystallite sizes of different films is attributed to the density of nucleation sites during the film growth, which, in turn, is influenced by the Mo doping concentration. The unit cell parameters listed in Table 1 are found to be in close agreement with those described in JCPDS Card No. 71-0131 ($a = 7.341$ Å, $b = 7.570$ Å, and $c = 7.754$ Å). A little variation observed in the unit cell parameters upon Mo doping is attributed to incorporation of molybdenum into WO_3 lattice network as the ionic radii of W^{6+} and Mo^{6+} are different.

3.1.2 SEM analyses

Figure 2a–d presents the SEM micrographs and the corresponding EDX profiles of the WO_3 films. The undoped

Table 1 Structural parameters of undoped and Mo-doped o-WO_3 films

Samples	Three most intense peaks		Lattice strain	Average crystallite size (nm)	Unit cell parameters (Å)	Unit cell volume (Å)
	d-spacing (Å)	(hkl)				
Undoped o-WO_3 film	3.65724	(200)	0.0078	13	$a = 7.315$	416.9
	2.62896	(220)	0.0137		$b = 7.563$	
	2.15604	(222)	0.0088		$c = 7.536$	
					$\alpha = \beta = \gamma = 90°$	
1 at% Mo-doped o-WO_3 film	3.6584	(200)	0.0078	17	$a = 7.317$	416.9
	2.63219	(220)	0.0082		$b = 7.580$	
	2.15607	(222)	0.0066		$c = 7.517$	
					$\alpha = \beta = \gamma = 90°$	
2 at% Mo-doped o-WO_3 film	3.84698	(020)	0.0082	17	$a = 7.335$	429.1
	3.66732	(200)	0.0117		$b = 7.694$	
	2.61909	(220)	0.0082		$c = 7.603$	
					$\alpha = \beta = \gamma = 90°$	
5 at% Mo-doped o-WO_3 film	3.53927	(012)	0.0066	26	$a = 7.312$	425.6
	2.57042	(122)	0.0053		$b = 7.452$	
	1.75133	(133)	0.0026		$c = 7.810$	
					$\alpha = \beta = \gamma = 90°$	

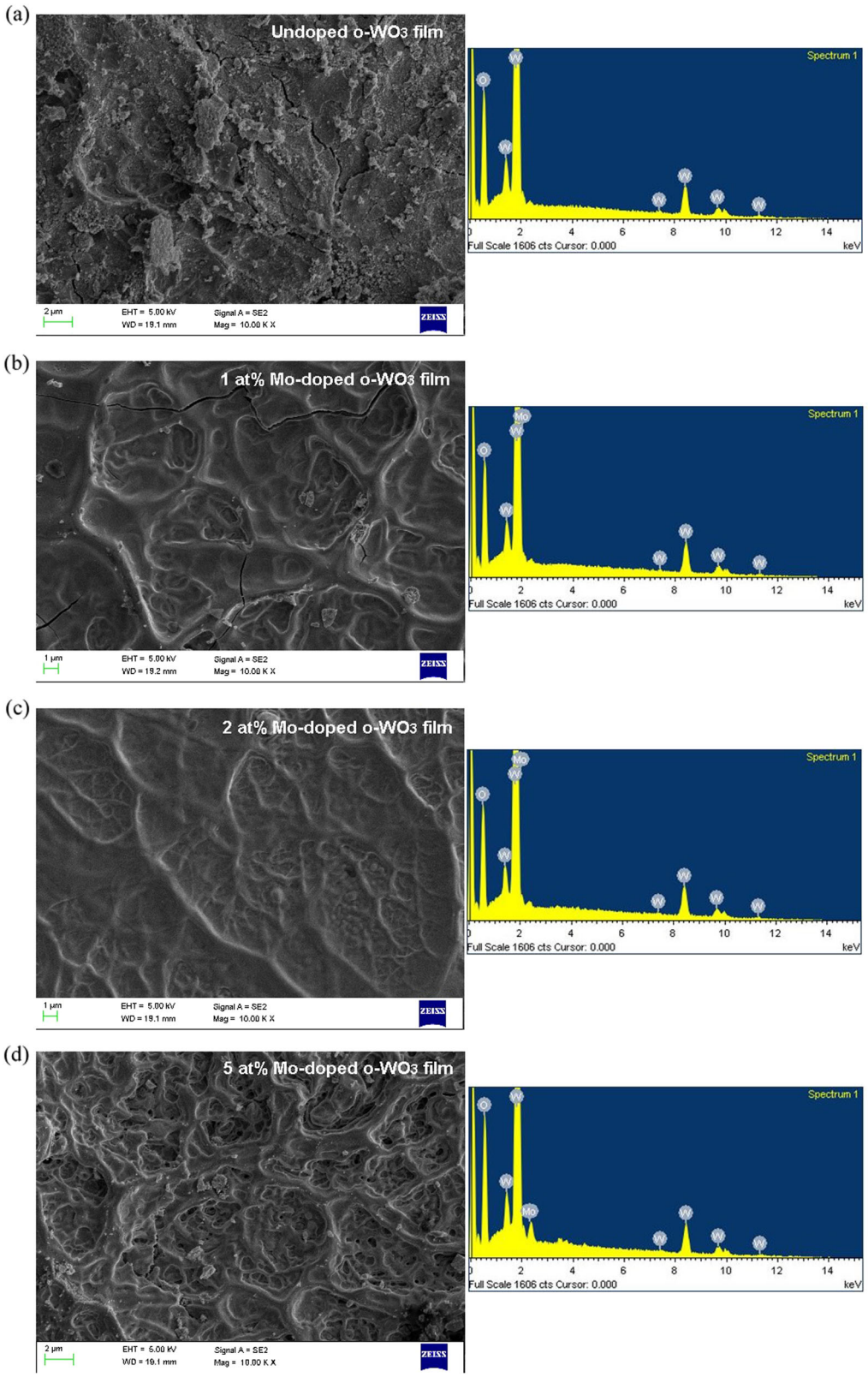

Fig. 2 a–d SEM images and the corresponding EDX profiles of the WO_3 films

Table 2 Topographical parameters of undoped and Mo-doped o-WO_3 films

Samples	Image surface area (μm^2)	Image projected surface area (μm^2)	Root mean square roughness, R_q (nm)	Average roughness, R_a (nm)
Undoped o-WO_3 film	113	100	207	168
1 at% Mo-doped o-WO_3 film	120	100	408	345
2 at% Mo-doped o-WO_3 film	104	100	88.2	73
5 at% Mo-doped o-WO_3 film	132	100	317	262

WO_3 film exhibits island-like morphology comprising of tiny grains. With the addition of molybdenum in WO_3, the morphology of film is changed. Upon 1 at% Mo doping, the film presents interweaved nest-like morphology. With the increase of doping to 2 at%, the morphology changes to root-like architecture. On further enhancement to 5 at% Mo doping, the film presents densely interweaved nest-like morphology. The enhanced interweaved-channels in 5 at% Mo-doped film provide sufficient pathways for easy diffusion of ions into the film network and faster kinetics which improve the electrochromic performance of the films. The EDX profiles confirm the presence of elements W and O in the undoped film, and W, Mo, and O in the doped films.

3.1.3 AFM analyses

Two- and three-dimensional AFM images, depicted in Fig. 3a–d, of the WO_3 films have been analysed using the Nanoscope Analysis software. The topographical parameters, viz., image surface area, image projected surface area, root mean square roughness (R_q) and average roughness (R_a) of the films thus obtained are listed in Table 2. As evident from the Table 2, among all the films, the image surface area is maximum for the 5 at% Mo-doped film, implying that the topography of the film is optimal for improved electrochromic performance. Further, the values of R_q and R_a are maximum for the 1 at% Mo-doped film followed by those of 5 at% Mo-doped film. This may arise due to more number of nucleation sites available during the time of film growth in the case of 5 at% Mo-doped film relative to that available in the 1 at % doped film; which is in agreement with the topographies of these films [Fig. 3(b, d)].

3.2 UV–visible spectroscopy studies

Optical transmission spectra of the WO_3 films deposited onto glass substrates are shown in Fig. 4. It has been found that all the films exhibit high transmittance varying between 65% and 75% in the visible range. Because of different film morphologies (surface roughness), there is a variation in transmittance arising out of the scattering of light [27]. Shifting of the absorption edge towards longer wavelength upon Mo doping implies decrease in the band gap energy. The optical band gap energies have been determined using the well-known Tauc's equation [28]:

$$\alpha h\nu = K\left(h\nu - E_g\right)^p \tag{5}$$

where K is a constant, E_g is the band gap energy of the semiconductor, α is the absorbance coefficient, and the values of exponent p depend upon the nature of band transition ($p = ½$ for direct transition, and $p = 2$ for indirect transition).

Having the reports of both direct and indirect transitions occurred in WO_3 [22, 29], the band gap energy value has been determined for both types of transitions. The direct band gap energy has been determined by extrapolating the linear portion of the $(Ah\nu)^2$ versus $h\nu$ plots to the energy-axis, shown in Fig. 5. Inset of Fig. 5 presents the plot of $(Ah\nu)^2$ versus $h\nu$ of 1 at% Mo-doped film in the extended ordinate. The direct band gap energies thus obtained are in the range of 3.50–3.56 eV. The direct band gap energy values of WO_3 films depend upon the crystallinity of the films, and can be found in the range of 3.27–3.65 eV [30]. The indirect band gap energy has been estimated from the linear extrapolations of the plots of $(Ah\nu)^{1/2}$ versus $h\nu$ to the energy-axis, shown in Fig. 6. Variation in the indirect band gap energies arises owing to the formation of allowed energy states in the band gap region of WO_3. In general, semiconducting materials may have direct or indirect band gap depending upon their crystal structures which are influenced by the preparative conditions. But in some cases, a material may have the both if it has a partial crystalline nature or is under the application of strain. Sharon et al. [31] have also reported both direct and indirect band gap energies for orthorhombic WO_3 film prepared by the vacuum evaporation technique.

3.3 Electrochromic studies

The basic mechanism involved in electrochromism is the phenomenon of charge transport in the crystal lattice. WO_3 thin film with tungsten sites as oxidation state W^{+6} is colourless in nature. Owing to insertion of charges during electrochemical reaction, W^{+6} are reduced to W^{+5} states,

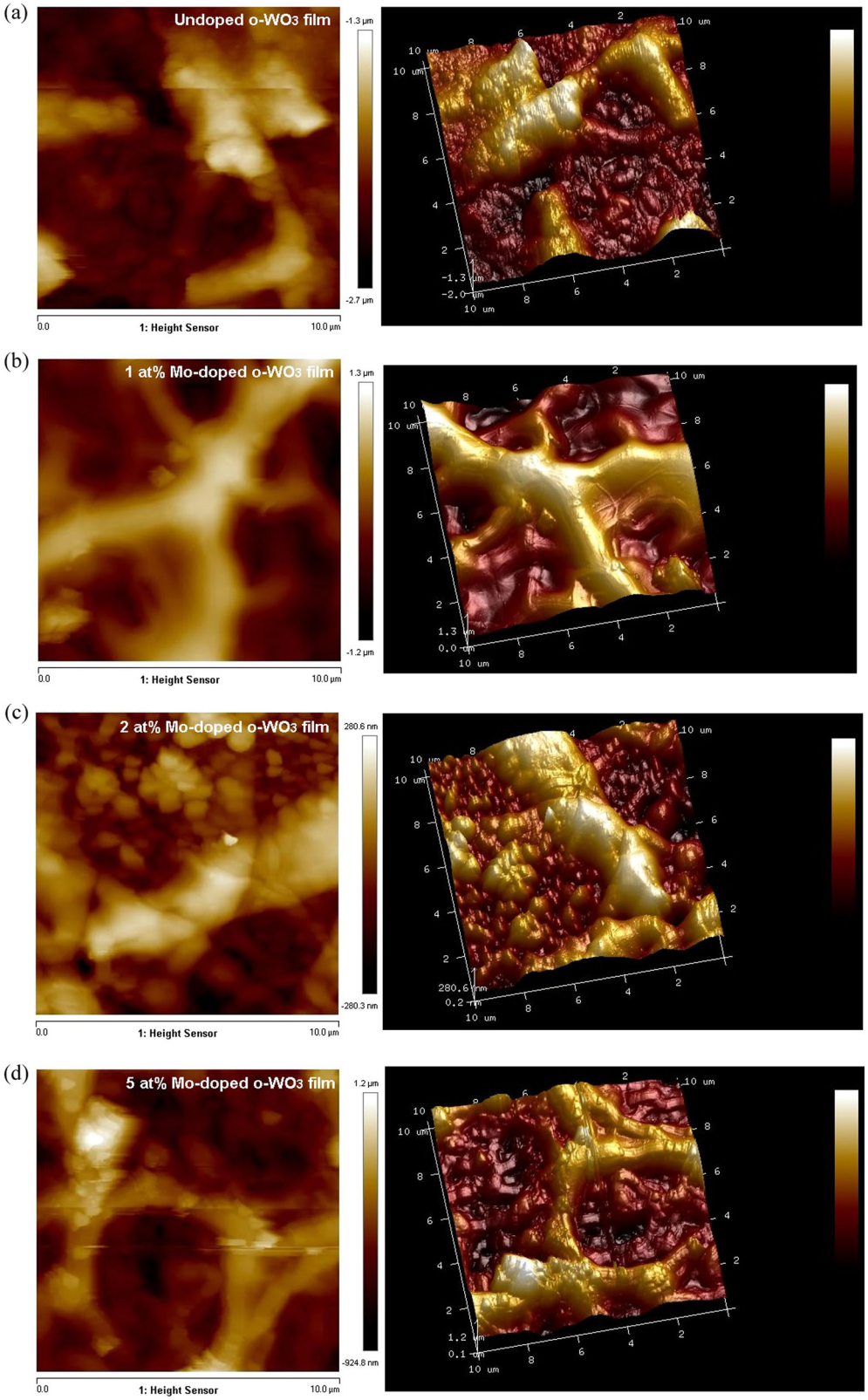

Fig. 3 a–d Two-dimensional and three-dimensional AFM images of the WO_3 films

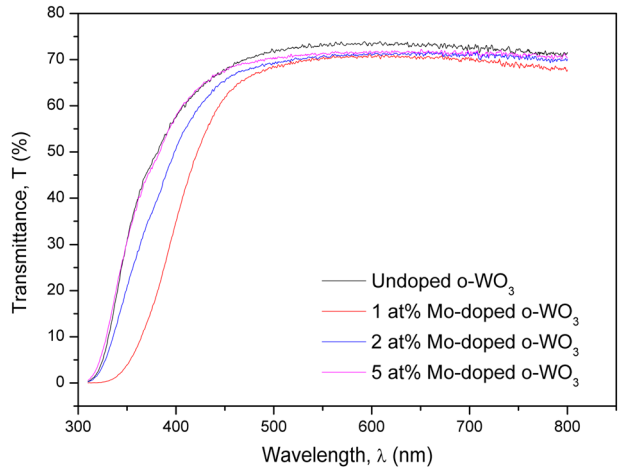

Fig. 4 Optical transmission spectra of the WO_3 films

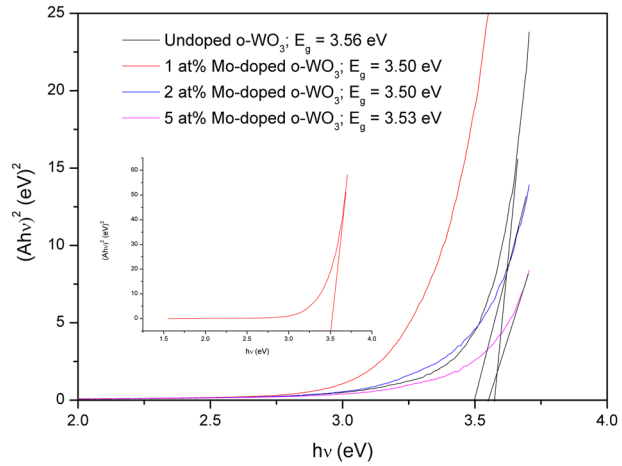

Fig. 5 Plot of $(Ah\nu)^2$ versus $h\nu$

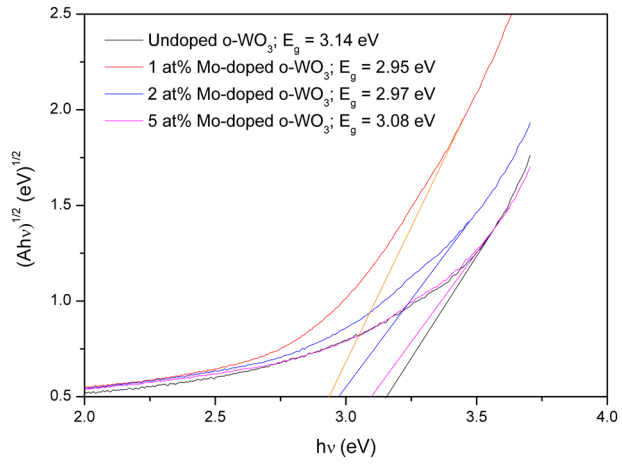

Fig. 6 Plot of $(Ah\nu)^{1/2}$ versus $h\nu$

giving blue coloration to the film. On electrochemical oxidation, W^{+6} sites are generated, changing blue coloration in the film to colourless. It has been widely accepted that insertion and extraction of electrons and metal ions (H^+, Li^+, etc.) in the crystal lattice play an important role in electrochromism. The electrochemical redox reaction involving coloration and bleaching phenomena in WO_3 thin films can be written as [32]:

$$WO_3(\text{colourless}) + xM^+ + xe^- \leftrightarrow M_xWO_3(\text{blue}) \quad (6)$$

where $M^+ = H^+$, Li^+, etc. M_xWO_3 is, in general, called as tungsten bronze. The subscript x in the formula M_xWO_3 represents the fractional number of sites, called the insertion coefficient, which are filled in the WO_3 lattice. At low x, intervalence charge transfer between W^{+5} and W^{+6} adjacent states results in blue coloration to the film. At higher x, the inserted ions expand the lattice of WO_3, whereas the compensating electrons enter the extended states of conduction band and thus alter its electronic structure which, in turn, affects its optical properties [1]. The electrochromic behaviour of the WO_3 films has been investigated by analysing the results of cyclic voltammetry (CV), Chronoamperometry, and impedance spectroscopy measurements.

3.3.1 Cyclic voltammetry

To investigate the cathodic/anodic behaviour of the WO_3 films, CV measurements were performed in the potential region of + 0.7 V to − 0.7 V at four different scan rates viz. 10, 20, 50, and 100 mV/s in the electrolyte of 0.1 M H_2SO_4. The cyclic voltammograms of the films thus measured are depicted in Fig. 7. Usually, when the WO_3 film electrodes are cathodically polarised, they have a progressive increase in the blue coloration with increasing cathodic potential. When the blue film electrodes are anodically polarised, they are bleached and almost colourless. During cathodic scan, as the potential is decreased, the current density goes on decreasing and attains a maximum negative value at the potential of − 0.7 V, corresponding to deep blue coloration to the film. This process is associated with the insertion of electrons and H^+ ions into the WO_3 films, resulting in the reduction of W^{+6} to W^{+5} states. During anodic scan, with the increase of potential, the current density goes from negative value to a maximum positive value and then decreases, corresponding to bleaching of the films. This is associated with the extraction of intercalated charges from the film structure, leading to the oxidation of $W^{+5} \rightarrow W^{+6}$. As evident from the cyclic voltammograms, all the films show a well-defined broad anodic peak during anodic scan, whereas a spike instead of a peak is observed at the potential of − 0.7 V during cathodic scan. Non-appearance

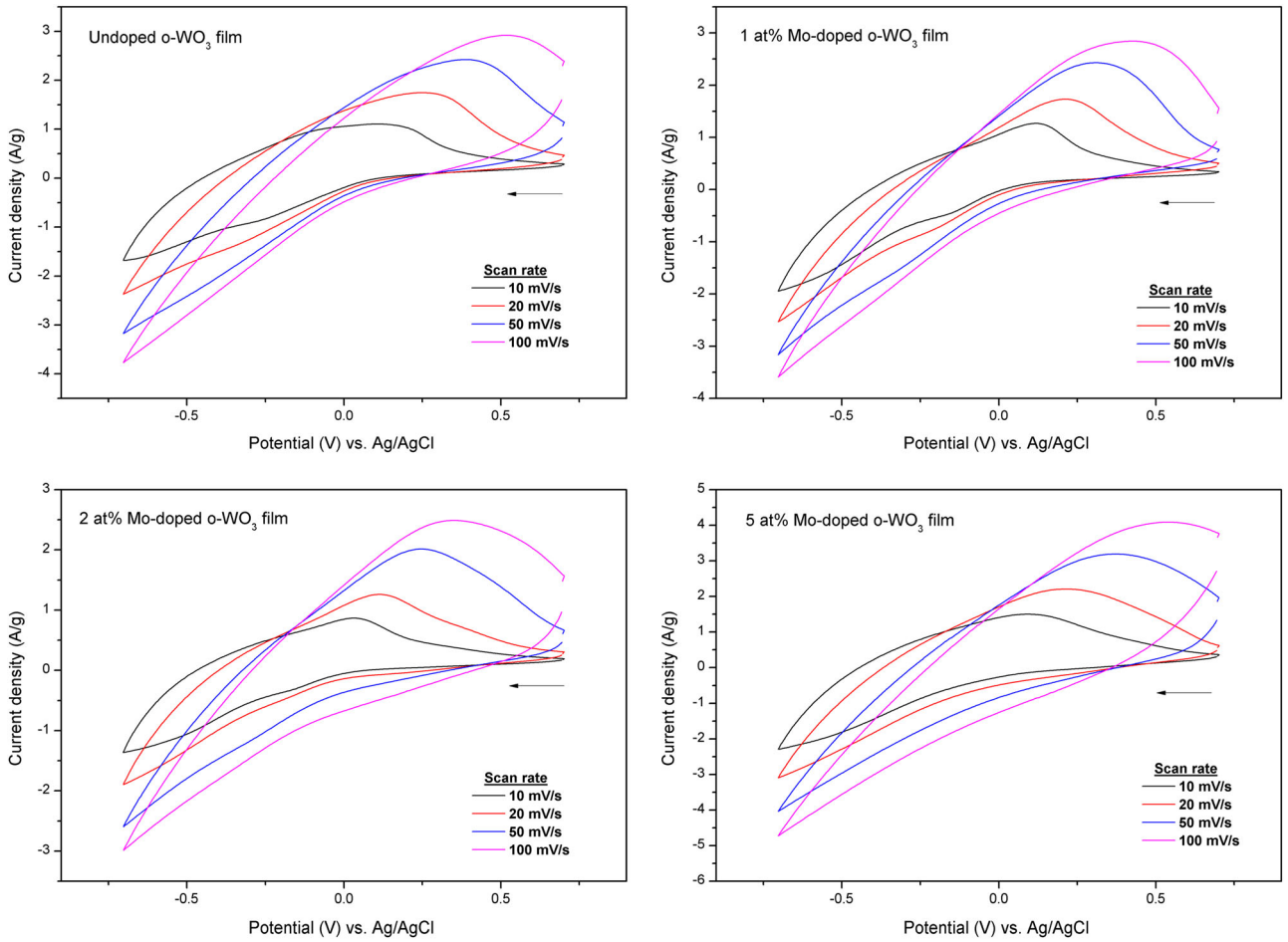

Fig. 7 Cyclic voltammograms of the WO_3 films. Arrow indicates the scan direction

of a well-defined peak in cathodic region is attributed to the back electromotive force formed within the tungsten bronze during ion insertion [33]. As shown in Fig. 7, the cathodic and anodic peak current densities are found to have the highest values for the WO_3 film doped with Mo concentration of 5 at%.

It has been found that for each film the anodic peak current density increases with the increasing scan rate and also shifts towards the higher potential. Shifting of anode peak position towards higher potential indicates that the change from coloured to bleached state is slower at higher scan rates [21]. This may be attributed to slower electron exchange kinetics at higher scan rates. The cathodic peak (spike) current density also rises with the increase of scan rate. The increase in cathodic and anodic peak current densities at higher scan rates is due to enhanced extent of H^+ ions insertion and extraction in the WO_3 film structure [34, 35]. Furthermore, the increased area of cyclovoltammetric curve with the increasing scan rate indicates larger amount of charge exchange during redox reaction at higher scan rates.

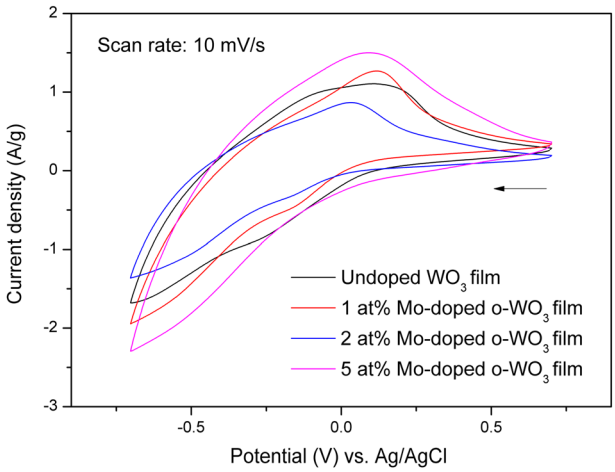

Fig. 8 Comparison of cyclic voltammograms of the WO_3 films at the scan rate of 10 mV/s. Arrow indicates the scan direction

Figure 8 presents the cyclic voltammograms of all the films recorded at a particular scan rate of 10 mV/s. Except for the case of 2 at% Mo doping, the cathodic and anodic peak current density increases for the WO_3 films doped with

1 at and 5 at% Mo. This indicates high capability of charge insertion and extraction for the film structure [36]. Also the anodic peak potential shifts towards the lower potential relative to that observed in the undoped WO_3 film. This indicates that the change from coloured to bleached state is faster for the WO_3 films doped with Mo. This is closely related to the microstructural features of the films. Among all the films, the area of cyclovoltammetric curve of the 5 at% Mo-doped WO_3 film has been found to be maximum [Fig. 8], signifying the greatest amount of charge exchange taking place in the film during electrochemical redox reaction. This reveals that insertion and extraction of H^+ ions are enhanced in WO_3 film doped with 5 at% Mo.

The extent of insertion and extraction of H^+ ions into the WO_3 host lattice can be studied by calculating the diffusion coefficient using Randles–Sevcik equation [37, 38]:

$$J_p = 2.72 \times 10^5 C\sqrt{n^3 D\nu} \tag{7}$$

where J_p is the peak current density in A/cm^2, n is the number of electrons involved in the redox process (it is assumed to be 1), D is the diffusion coefficient in cm^2/s, C is the concentration of active ions in the electrolyte solution in mol/cm^3, and ν is the scan rate in V/s. The diffusion coefficients thus obtained are listed in Table 3. It has been found that there is a variation in the diffusion constant values upon Mo doping, which could be due to variation in the mobility of the diffusing ionic species (H^+) in the redox reaction. The mobility of the H^+ ions in the film is influenced greatly by the microstructural features of the film.

To calculate the coloration efficiency of the WO_3 films, the optical transmittance spectra of the coloured (with the application of cathodic potential of -0.7 V) and bleached (with the potential of $+0.7$ V) states of the films were recorded, and are shown in Fig. 9. The change in optical density (Δ OD) has been determined from the optical transmittances of coloured ($T_{coloured}$) and bleached ($T_{bleached}$) films using the relation:

$$\Delta \mathrm{OD}(\lambda) = \ln\left(\frac{T_{bleached}}{T_{coloured}}\right) \tag{8}$$

Coloration efficiency (η) defined as the ratio of the change in optical density to the amount of charge intercalated, has been determined by the relation [39]:

$$\eta(\lambda) = \frac{\Delta OD(\lambda)}{Q/A} \tag{9}$$

where A is the electrode area of the film and Q is the amount of charge intercalated which is derived from the CV measurements [9, 38]. Figure 10 presents the plot of change

Table 3 Electrochromic properties of undoped and Mo-doped o-WO_3 thin films

Samples	Cyclic voltammetry measurements						Chronoamperometry measurements		
	Scan rate (mV/s)	Cathodic current density (A/cm^2)	Anodic current density (A/cm^2)	Diffusion coefficient (cm^2/s)		Colouration efficiency at 550 nm (cm^2/C)	Charge intercalated (C/g)	Charge extracted (C/g)	Reversibility (%)
				$D_{insertion}$	$D_{extraction}$				
Undoped o-WO_3 film	10	0.0024	0.0016	7.78E-11	3.37E-11	14.1	55.72	38.54	69.2
	20	0.0034	0.0025	7.74E-11	4.20E-11				
	50	0.0054	0.0035	7.77E-11	3.23E-11				
	100	0.0054	0.0042	3.92E-11	2.35E-11				
1 at% Mo-doped o-WO_3 film	10	0.0029	0.0019	1.14E-10	4.86E-11	16.6	53.61	35.92	67.0
	20	0.0038	0.0026	9.70E-11	4.53E-11				
	50	0.0047	0.0036	6.05E-11	3.57E-11				
	100	0.0054	0.0043	3.90E-11	2.44E-11				
2 at% Mo-doped o-WO_3 film	10	0.0020	0.0013	5.48E-11	2.21E-11	14.9	39.23	27.5	70.1
	20	0.0028	0.0019	5.29E-11	2.34E-11				
	50	0.0038	0.0030	3.97E-11	2.39E-11				
	100	0.0044	0.0037	2.63E-11	1.82E-11				
5 at% Mo-doped o-WO_3 film	10	0.0024	0.0016	7.81E-11	3.34E-11	43.3	71.78	51.95	72.4
	20	0.0032	0.0023	7.12E-11	3.62E-11				
	50	0.0042	0.0033	4.83E-11	3.02E-11				
	100	0.0050	0.0043	3.31E-11	2.48E-11				

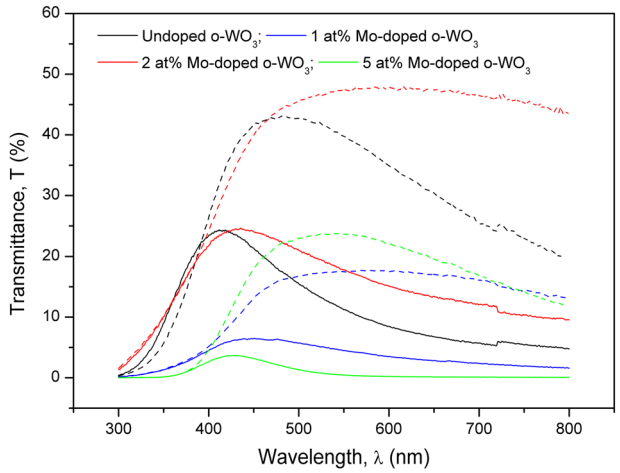

Fig. 9 Optical transmittance spectra of the coloured and bleached states of the WO_3 films. Solid and dashed lines represent the coloured and bleached states, respectively

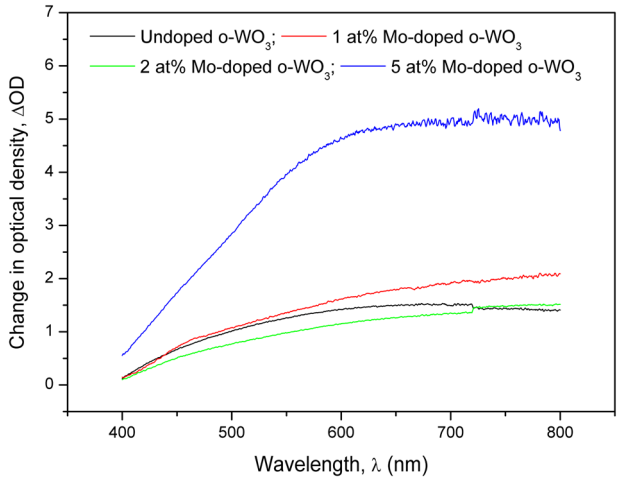

Fig. 10 Plot of change in optical density, ΔOD, versus wavelength, λ, of the WO_3 films

in optical density, ΔOD, versus wavelength, λ, of the WO_3 films, whereas plot of the amount of charge intercalated per unit area, Q/A, versus Mo-dopant concentration is depicted in Fig. 11. It has been found that the coloration efficiency of the WO_3 film improves upon Mo doping, having the highest value 43.3 for the doping of 5 at% Mo. This evinces that the structure of 5 at% Mo-doped WO_3 film provides an easy way to diffusion and charge transfer process of ions.

The electrochemical stability of the WO_3 films has been examined by repeating reduction–oxidation cycles between the sweep potential range from + 0.7 V to − 0.7 V several times at the scan rate of 50 mV/s [Fig. 12]. In all the films, the nature of the cyclovoltammetric curves remains almost unchanged even after 100 reduction–

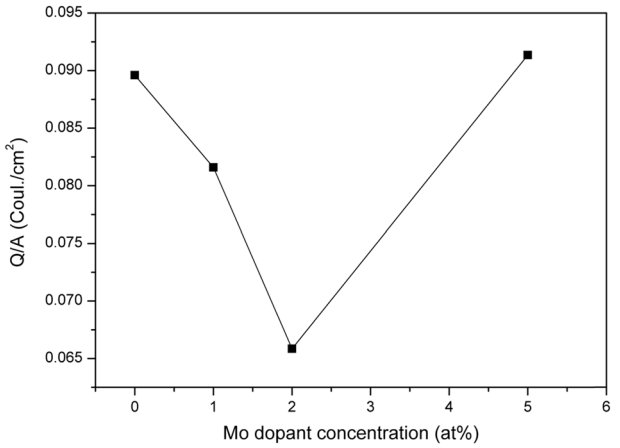

Fig. 11 Plot of the amount of charge intercalated per unit area, Q/A, versus Mo dopant concentration

oxidation cycles, thus establishing good electrochemical stability of the films.

3.3.2 Chronoamperometry

Chronoamperometry measurements were carried out for 10 cycles with the potential being stepped between − 0.7 V and + 0.7 V vs. Ag/AgCl for 25 s, and are shown in Fig. 13. Here, we only present the first three cycles to avoid clustering of data in the figure. In the time interval 0–25 s, the film was in coloured state while in the next time interval 25–50 s the film was in bleached state. As evident from the Fig. 11, in 5 at% Mo-doped film, on applying the potential of − 0.7 V, the current density remains constant for a considerable time and then begins to decrease. This leads to infer that in the beginning for a considerable time, there is no potential barrier formed at the WO_3-electrolyte interface; as a result the current density arising due to insertion of H^+ ions into the film remains almost constant. Later on, a progressive potential barrier at the WO_3-electrolyte interface is formed, resulting in a decrease in current. Further, during oxidation cycle, on applying the potential of + 0.7 V, the current density remains constant for some time and thereafter begins to fall. Therefore, it is inferred that during bleaching, in the beginning for some time, the extraction of H^+ ions from the bulk of the film is not governed by the space-charge. The WO_3 film doped with 5 at% Mo exhibits fastest switching response. In general, the coloration process is slower than the bleaching in WO_3 films owing to faster bleaching kinetics [17].

The reversibility of the films, defined as the ratio of the charge extracted to the charge intercalated in the film, is listed in Table 3. The values of charge intercalated and charge extracted are obtained from the integration of the

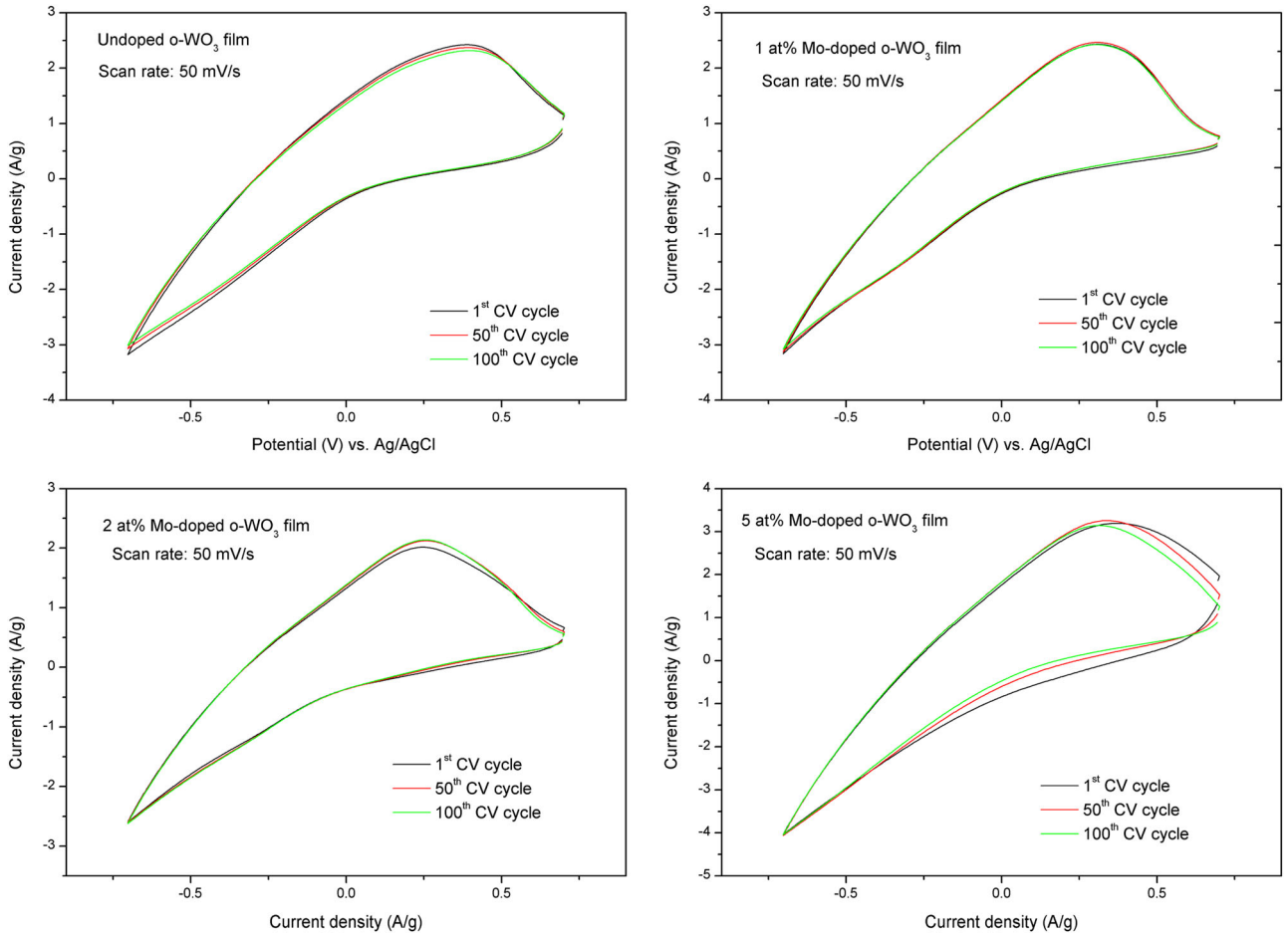

Fig. 12 Electrochemical stability of the WO_3 films

cathodic and anodic current densities. It has been found that the reversibility is optimal for the film with 5 at% Mo doping. Considering the reversibility and the switching response from chronoamperometry and the coloration efficiency from cyclic voltammetry it has been concluded that the 5 at% Mo-doped WO_3 film has an optimal electrochromic response.

3.3.3 Electrical impedance spectroscopy

Figure 14 presents the Nyquist plots in the frequency range of 10 kHz–1 Hz, comprising of the real versus the imaginary component of the electrical impedance of the WO_3 films. The Bode plots comprising of the logarithm of the measured impedance (Z) and the phase angle, versus the logarithm of the frequency are depicted in Fig. 15. The Bode plots provide a good comparison of total impedance values for WO_3 films. The Nyquist impedance plots have been analysed using Nova software, taking into consideration the equivalent circuit shown in the inset of Fig. 12, and the fitted parameters are listed in Table 4. In the equivalent circuit, R_s corresponds to the electrolyte resistance; R_{film} and C_{film} are the resistance and capacitance of the WO_3 film, respectively; R_{ct} is the charge transfer resistance at the electrolyte/electrode interface, signifying how beneficial is the film morphology for proton transfer; W is the Warburg diffusion impedance (ionic diffusion in the film electrode), and C_{dl} is the capacitance of WO_3/electrolyte interface [40]. Mathematically, Warburg impedance is expressed as: $W = 1/[Y_o\ (j\omega)^{0.5}]$, where Y_o is the admittance ($1/\ |Z|$) at $\omega = 1$ rad/s. Among all the circuit elements, the charge transfer resistance is the most important element of the circuit, closely linked to the electrochromic behaviour of the films. The charge transfer resistance is the resistance offered to the process of electrons from the film electrode to the H^+ ions in the liquid phase, and therefore it should have low value for films showing good electrochromic properties [41, 42]. Goodness of fit, χ^2, in impedance spectroscopy is also included in Table 4. The lower values of chi-square support the best fit of Nyquist plots. As evident from Table 4, the

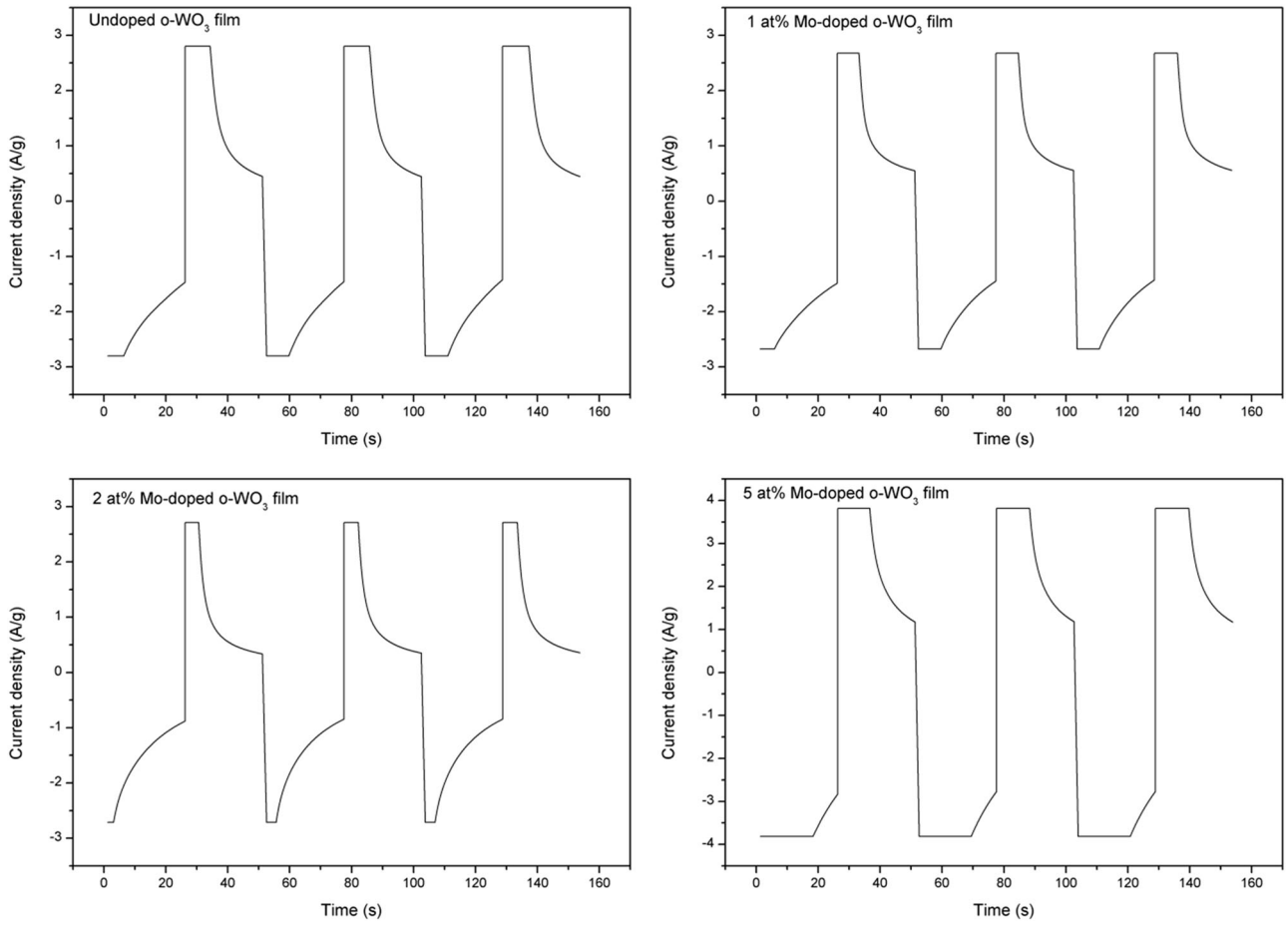

Fig. 13 Chronoamperometry curves of the WO_3 films

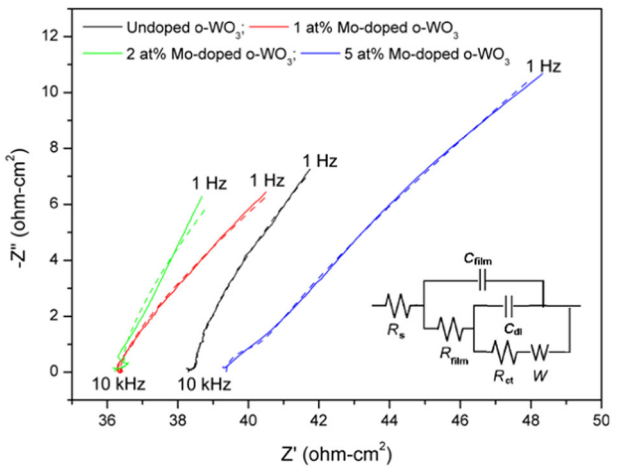

Fig. 14 Nyquist impedance plots of the WO_3 films. Solid and dashed lines represent the experimental and fitted data, respectively. Inset of Fig. 12 represents the equivalent circuit fitting

charge transfer resistance is least for the 5 at% Mo-doped WO_3 film. That is why during chronoamperometry measurements [Fig. 13], on applying the cathodic potential, the current density remains constant for a considerable time in the case of 5 at% Mo-doped film.

A comparison of this work with those for other dopants in WO_3-based films/devices reported earlier in literature is presented in Table 5.

4 Conclusions

All the as-prepared films possess orthorhombic phase of WO_3. With varying Mo-doping concentrations, the morphologies of films change. Three-dimensional AFM image analyses show that the 5 at% Mo-doped film has the maximum image surface area. The optical direct band gap energies of WO_3 films have been found to be in the range of 3.50–3.56 eV. Among all the films, WO_3 doped with 5 at% Mo exhibits fastest switching response and highest colouration efficiency. It has been concluded that the spray-pyrolysed 5 at% Mo-doped WO_3 films have an optimal electrochromic performance, and therefore have the potential to be used as an effective electrochromic material for smart window applications.

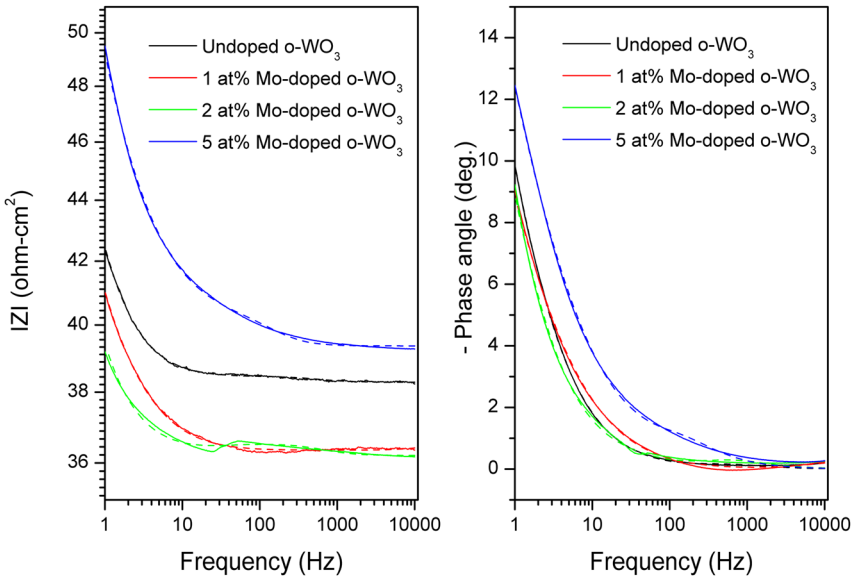

Fig. 15 Bode plots of the WO_3 films. Solid and dashed lines represent the experimental and fitted data, respectively

Table 4 Equivalent circuit fitting parameters of the Nyquist impedance plots of the o-WO_3 films

Samples	R_S (Ω-cm^2)	C_{film} ($\times 10^{-6}$/Fcm^2)	R_{film} ($\times 10^{-3}$ Ω-cm^2)	R_{ct} ($\times 10^{-9}$ Ω-cm^2)	$W(\Omega cm^{2/}s^{0.5})/Y_o$ ($\times 10^{-3}$ Ω/cm^2)	C_{dl} ($\times 10^{-3}$/Fcm^2)	χ^2
Undoped o-WO_3 film	38.3	1400	222	1.33×10^9	29.7	9.39	0.00048
1 at% Mo-doped o-WO_3 film	36.7	24.6	314	3.54×10^8	41.0	6.43	0.001
2 at% Mo-doped o-WO_3 film	36.2	694	375	2.60×10^9	33.5	9.08	0.0025
5 at% Mo-doped o-WO_3 film	39.4	843	1520	89.9	25.3	2.16	0.0023

Table 5 Electrochromic response of different dopants in WO_3-based films/devices

WO_3-based films/devices	Deposition/preparation method	Electrochromic response	Reference
Mo-doped WO_3 thin films	Spray pyrolysis technique	Coloration efficiency at 550 nm improves from 14.1 to 43.3 cm^2/C, and reversibility also improves from 69.2 to 72.4% for the 5 at% Mo-doped film.	This work
V-doped WO_3 thin films	Reactive dc magnetron sputtering	Coloration efficiency decreases with increasing vanadium content.	[10]
Gd-doped WO_3 films	RF magnetron sputtering technique	High coloration efficiency (68.3 cm^2/C) at 633 nm and fast switching response are observed in 0.9 wt.% Gd-doped film.	[15]
Ti-doped WO_3 films	Sol–gel technique	Electrochromic performance is enhanced by small doping concentration of titanium.	[16]
Nb-doped WO_3 films	Pulsed spray pyrolysis technique	Reversibility improves from 75 to 92% for the 6 at% Nb-doped film but coloration efficiency decreases from 25 to 7 cm^2/C.	[17]
Ni_xW_{1-x} oxide films	DC magnetron co-sputtering technique	Coloration efficiency improves for films with $0.10 < x < 0.15$.	[18]
Ru-doped WO_3 thin films	DC magnetron co-sputtering technique	Electrochromic properties are affected by the presence of Ru ions.	[19]
Mo-doped WO_3 thin films	Spray pyrolysis technique	Best electrochromic response is observed in 6 at% Mo-doped fim.	[20]
Mo-doped WO_3 thin films	RF magnetron sputtering technique	High coloration efficiency of ~ 42.5 cm^2/C is observed for the 1.3 at% Mo-doped film.	[21]

Acknowledgements We express our gratitude to Centre for Interdisciplinary Research, MNNIT Allahabad, India for providing XRD and UV–Vis measurements, and Sophisticated Analytical Instrument Facility, Indian Institute of Technology Bombay, India for SEM and AFM characterisation facilities.

Compliance with ethical standards

Conflict of interest The authors declare that they have no conflict of interest.

Publisher's note: Springer Nature remains neutral with regard to jurisdictional claims in published maps and institutional affiliations.

References

1. Somani PR, Radhakrishnan S (2002) Mater Chem Phys 77:117
2. Granqvist CG (1995) Handbook of Inorganic Electrochromic Materials, Elsevier, Amsterdam
3. Kahl JL, Faulkner LR, Dwarakanath K, Tachikawa H (1986) J Am Chem Soc 108:5434
4. Honda K, Ochiai J, Hayashi H (1986) J Chem Soc Chem Commun 1:168
5. Bruinink J (1976) Electrochromic display devices. In: Kmetz AR, VonWilli FK (Eds.) Non-emissive Electro-optic Displays. Plenum Press, New York
6. Bernard MC, Goff AH-L, Zeng W (1998) Electrochem Acta 44:781
7. Kostis I, Vasilopoulou M, Soultati A, Argitis P, Konofaos N, Douvas AM, Vourdas N, Papadimitropoulos G, Davazoglou D (2013) Microelectron Eng 111:149
8. Bhosale NY, Mali SS, Hong CK, Kadam AV (2017) Electrochim Acta 246:1112
9. Li C, Hsieh JH, Hung M-T, Huang BQ (2015) Thin Solid Films 587:75
10. Karuppasamy KM, Subrahmanyam A (2008) J Phys D: Appl Phys 41:035302. 6pp
11. Rougier A, Portemer F, Quede A, Marssi ME (1999) Appl Surf Sci 153:1
12. Wang Z, Hu X (2001) Electrochim Acta 46:1951
13. Ozer N, Lampert CM (1999) Thin Solid Films 349:205
14. Hepel M, Redmond H, Dela I (2007) Electrochim Acta 52:3541
15. Yin Y, Lan C, Hu S, Li C (2018) J Alloy Compd 739:623
16. Paipitak K, Techitdheera W, Porntheeraphat S, Pecharapa W (2013) Energy Procedia 34:689
17. Bathe SR, Patil PS (2007) J Phys D: Appl Phys 40:7423
18. Green SV, Pehlivan E, Granqvist CG, Niklasson GA (2012) Sol Energy Mater Sol Cells 99:339
19. Cazzanelli E, Castriota M, Kalendarev R, Kuzmin A, Purans J (2003) Ionics 9:95
20. O-Rueda de León JM, Acosta DR, Pal U, Casta˜neda L (2011) Electrochim Acta 56:2599
21. Madhavi V, Kumar PJ, Kondaiah P, Hussain OM, Uthanna S (2014) Ionics 20:1737
22. Mukherjee R, Kushwaha A, Sahay PP (2014) Electron Mater Lett 10:401
23. Mukherjee R, Prajapati CS, Sahay PP (2014) J Therm Spray Technol 23:1445
24. Rajagopal S, Nataraj D, Mangalaraj D, Djaoued Y, Robichaud J, Khyzhun OY (2009) Nanoscale Res Lett 4:1335
25. Muller U (1993) Inorganic Structural Chemistry. Wiley, Chichester
26. Wahab MA (2010) Solid State Physics. Narosa Publishing House, New Delhi
27. Beena D, Lethy KJ, Vinodkumar R, Pillai VPM, Ganesan V, Phase DM, Sudheer SK (2009) Appl Surf Sci 255:8334
28. Goswami A (2005) Thin Film Fundamentals, New Age International (P) Ltd., New Delhi
29. Asghari Z, Eshghi H (2017) J Electron Mater 46:1439
30. Deb SK (1973) Philos Mag 27:801
31. Sharon M, Sharan MK, Jawalekar SR (1984) Sol Energy Mater 10:329
32. Patil PS, Patil PR, Kamble SS, Pawar SH (2000) Sol Energy Mater Sol Cells 60:143
33. Patil PR, Pawar SH, Patil PS (2000) Solid State Ion 136–137:505
34. Sivakumar R, A. Raj ME, Subramanian B, Jayachandran M, Trivedi DC, Sanjeeviraja C (2004) Mater Res Bull 39:1479
35. Meenakshi M, Gowthami V, Perumal P, Sivakumar R, Sanjeeviraja C (2015) Electrochim Acta 174:302
36. Kalagi SS, Mali SS, Dalavi DS, Inamdar AI, Im H, Patil PS (2012) Electrochim Acta 85:501
37. Nicholson RS, Shain I (1964) Anal Chem 36:706
38. Mukherjee R, Sahay PP (2016) J Alloy Compd 660:336
39. Lu Y, Liu L, Mandler D, Lee PS (2013) J Mater Chem C 1:7380
40. Lee SH, Cheong HM, Tracy CE, Mascarenhas A, Pitts JR, Jorgensen G, Deb SK (2000) Appl Phys Lett 76:3908
41. Alsawafta M, Golestani YM, Phonemac T, Badilescu S, Stancovski V, Truong V-V (2014) J Electrochem Soc 161:H276
42. Mishra RK, Prajapati CS, Sahay PP (2018) J Alloy Compd 749:172